

A million-scale dataset and generalizable foundation model for nanomaterial-protein interactions

Hengjie Yu^{1,2}, Kenneth A. Dawson³, Haiyun Yang¹, Shuya Liu¹, Yan Yan^{3,4}, Yaochu Jin^{1,2*}

¹School of Engineering, Westlake University, Hangzhou, Zhejiang 310030, China

²Institute of Advanced Technology, Westlake Institute for Advanced Study, Hangzhou, Zhejiang 310024, China

³Centre for BioNano Interactions, School of Chemistry, University College Dublin, Belfield, Dublin 4, Ireland

⁴School of Biomolecular and Biomedical Science, UCD Conway Institute of Biomolecular and Biomedical Research, University College Dublin, Belfield, Dublin 4, Ireland

*Corresponding author: Yaochu Jin. E-mail: jinyaochu@westlake.edu.cn

Abstract: Unlocking the potential of nanomaterials in medicine and environmental science hinges on understanding their interactions with proteins, a complex decision space where AI is poised to make a transformative impact. However, progress has been hindered by limited datasets and the restricted generalizability of existing models. Here, we propose NanoPro-3M, the largest nanomaterial-protein interaction dataset to date, comprising over 3.2 million samples and 37,000 unique proteins. Leveraging this, we present NanoProFormer, a foundational model that predicts nanomaterial-protein affinities through multimodal representation learning, demonstrating strong generalization, handling missing features, and unseen nanomaterials or proteins. We show that multimodal modeling significantly outperforms single-modality approaches and identifies key determinants of corona formation. Furthermore, we demonstrate its applicability to a range of downstream tasks through zero-shot inference and fine-tuning. Together, this work establishes a solid foundation for high-performance and generalized prediction of nanomaterial-protein interaction endpoints, reducing experimental reliance and accelerating various *in vitro* applications.

Introduction

Nanomaterials have attracted significant attention due to their unique physical, chemical, and biological properties, playing an increasingly important role across diverse fields, including biomedicine¹, agriculture², environment³ and beyond. Understanding the interactions between nanomaterials and biological environments is essential for advancing their efficient and sustainable applications. Among these interactions, the spontaneous formation of the protein corona on nanomaterial surfaces can profoundly alter their physicochemical properties and biological behaviors⁴. However, the interaction between nanomaterials and protein is influenced by a multitude of factors^{5,6}, including the physicochemical properties of nanomaterials (such as size, surface charge, and concentration), the type of biological fluid involved (e.g., plasma, serum, or cerebrospinal fluid from human or mouse), and environmental parameters where nano-bio interactions happen (such as temperature, flow rate, and incubation time). In addition, protein corona isolation and proteomic characterization are highly sensitive to the experimental protocols and analytical methodologies employed^{7,8}. Given these complexities, experimental studies involving labor-intensive and costly characterization are fundamentally constrained in their ability to systematically probe multiple variables. These limitations highlight the need for scalable, data-driven approaches to elucidate the principles underlying protein corona formation and to enable accurate prediction of nanomaterial-protein interactions.

AI methods, with their capacity to model complex, nonlinear relationships, hold great promise for predicting protein corona composition. Early in 2018, one of the first machine learning (ML) models applied random forest (RF) classification to predict protein corona formation on silver nanoparticles, achieving high accuracy (F1 score = 0.81) based on nanoparticle, protein, and solution properties⁹. In 2020, a study built a dataset of 652 nanoparticle-protein interactions and developed 178 RF regression models to predict the relative protein abundance (RPA) of each protein, reaching correlation coefficient above 0.75¹⁰. Recent research further leveraged this dataset to

train traditional ML models capable of predicting RPA, and deployed the models¹¹ and dataset online available¹². In addition to predicting the affinity of specific proteins for different nanomaterials, RF classifiers have also been employed to predict the binding affinity of various proteins toward a given type of carbon nanotube, achieving an accuracy of 0.78¹³. However, these existing ML prediction tools are constrained by limited datasets and model architectures, typically offering predictive capabilities for only specific nanomaterials or proteins. This inherent lack of generalization to previously unseen nanomaterials or proteins limits the broader applicability and practical utility of such models.

Recent advancements in pre-trained models, such as protein language models (e.g., ESM2¹⁴ and AlphaFold 3¹⁵) and text embedding models (e.g. Linq-Embed-Mistral¹⁶ and BERT¹⁷), offer unprecedented opportunities to develop generalizable predictive frameworks. Protein language models have been applied to predict structure¹⁸, function¹⁹, and molecular interactions¹⁵ and to generate protein sequences²⁰. In contrast to conversational models like ChatGPT, text embedding models are specifically designed to generate dense numerical representations that capture the semantic content of entire texts, enabling efficient similarity comparisons and downstream learning, such as molecule entity understanding²¹ and materials discovery²². Trained on extensive and diverse datasets, these pre-trained models exhibit remarkable capacity to capture intricate semantic relationships, laying a robust foundation for generalizable learning. However, such advanced AI approaches have not yet been applied to the study of nanomaterial-protein interactions, where the lack of sufficient data remains a significant challenge. We therefore hypothesize that, given sufficiently comprehensive datasets, it is feasible to develop models capable of predicting nanomaterial-protein interactions in a generalized manner, thus overcoming the limitations inherent in current task-specific machine learning methods.

The contribution of this work is shown in Fig. 1. Here, we present NanoPro-3M, a

comprehensive dataset constructed by meticulously collecting and curating data from over 2,500 articles, resulting in more than 3.2 million samples encompassing over 37,000 unique proteins. Using the largest known dataset to date, we build NanoProFormer, a foundation model based on multimodal pre-trained representation learning, which enables generalizable predictions on samples with missing data, unseen nanomaterials, and unseen proteins. We further dissect the contributions and interactions of individual modalities and features and demonstrate their utility across diverse downstream applications. Moreover, building on the model’s strong generalization capabilities and recognizing its current limitations in endpoint-focused prediction, we propose future directions for both AI-assisted applications and foundational experimental research.

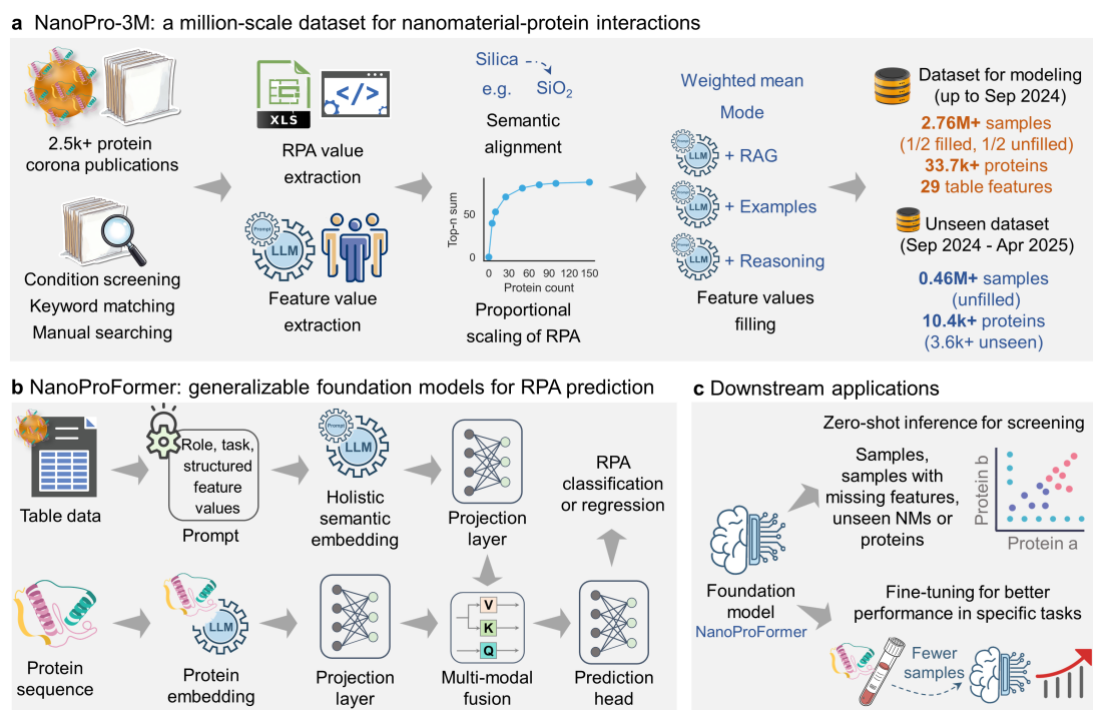


Fig.1: Contributions of this work. (a) The proposed NanoPro-3M dataset has the largest sample size and number of proteins known so far, laying the foundation for building a foundation model. It holds a role in the protein corona field analogous to that of ImageNet in computer vision. (b) NanoProFormer, a multimodal fusion foundation model built on protein- and text-based pretrained models, exhibits strong generalization capabilities across diverse prediction tasks. (c) Downstream applications of

NanoProFormer, via zero-shot inference and fine-tuning, are demonstrated on unseen samples and specific cases.

Results

Overview of NanoPro-3M dataset

As of September 20, 2024, we performed a comprehensive literature search across Web of Science, PubMed, and Scopus. With assistance from large language models (LLMs)²³, we extracted structured features from these studies, followed by manual verification. We collected a total of 29 features, including fourteen related to nanomaterial properties (e.g. core, surface modification, zeta potential, hydrodynamic diameter, and concentration), nine incubation conditions (e.g. protein source, culture media, temperature, time, and flow speed), five separation parameters (e.g. separation method and centrifugation parameters if centrifugation is used), and one proteomic analysis setting parameter (proteomic depth). Despite manual alignment of similar semantics, the dataset still comprises over 100 categories for nanoparticle core and incubation protein sources, and more than 200 categories for surface modifications, highlighting the substantial diversity and complexity of parameters involved in nanomaterial-protein interaction studies. RPA values were estimated using normalization methods based on available data. For studies with multiple experimental groups, protein counts were aggregated, and missing proteins were assigned an RPA of zero (called "local fill" method), resulting in 1.19 million samples. For studies reporting only top-ranked proteins, we applied top-n proportional scaling based on reference distributions from complete datasets (see Fig. 1a). Additionally, a "global fill" method was applied by assigning zero to commonly observed proteins not reported in specific studies, adding 190,000 samples. All included samples had at least one missing numerical feature. To address this, we employed a range of imputation strategies, including weighted means, modes, LLM with retrieval augmentation generation (RAG)²⁴, example-based LLM inference²⁵, and reasoning LLM²⁶. This process produced two datasets: a merged dataset containing both filled and raw samples (2.76

million samples), and a filled-only dataset (1.38 million samples). Moreover, protein sequences were retrieved from UniProt²⁷. The overview of the proposed dataset is shown in Fig. 2.

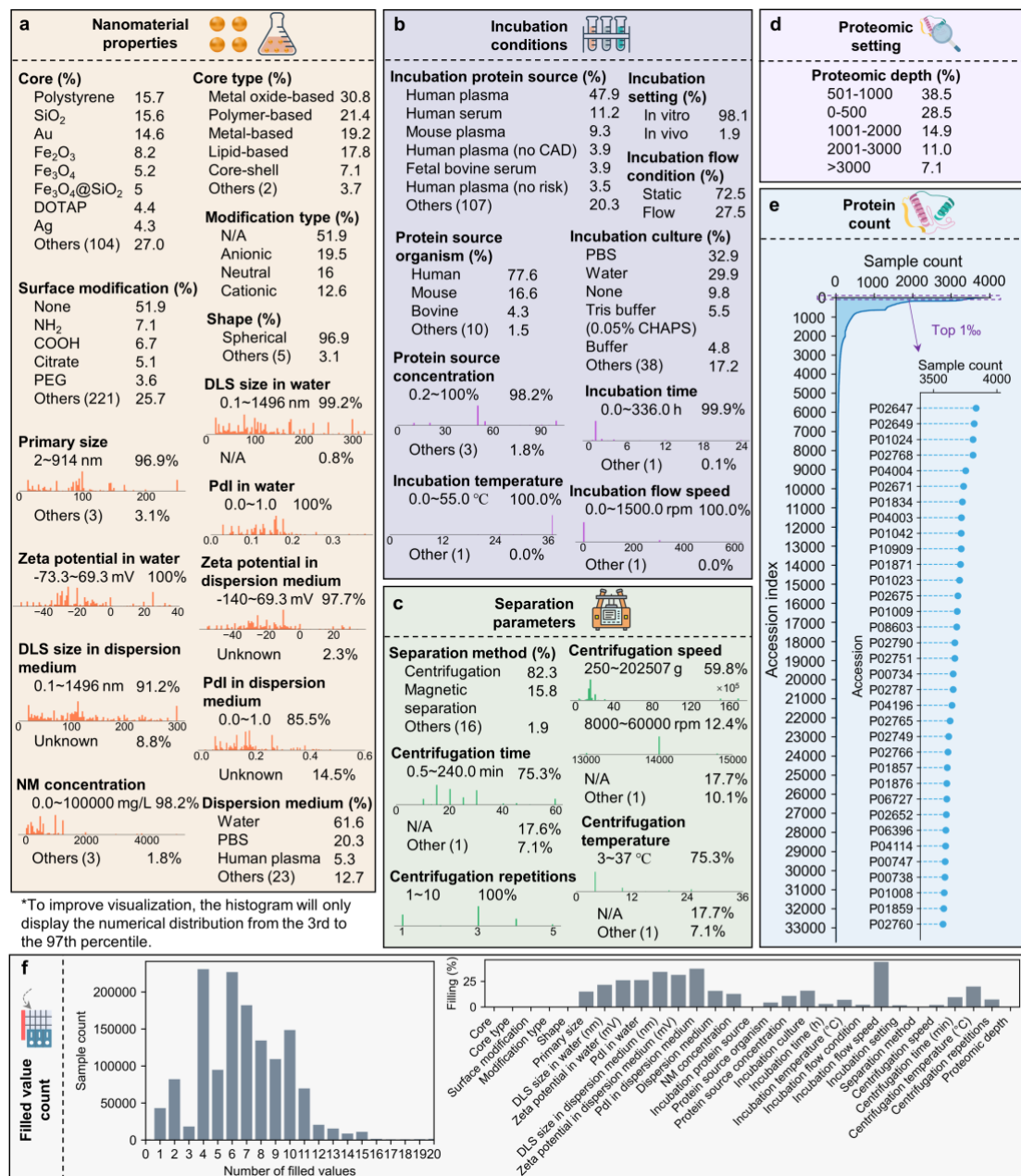


Fig.2: Overview of the proposed NanoPro-3M dataset for nanomaterial-protein interactions. Data distribution of (a) nanomaterial properties, (b) incubation conditions, (c) separation parameters, and (d) proteomic settings in the filled-only dataset. Note that numerical features may be represented differently across studies. (e) Summary of protein counts and (f) statistics on missing value fill in the merged dataset.

During model training, filled samples and their corresponding unfilled counterparts were confined to the same data split (training, validation, or test set). The dataset was partitioned in an 8:1:1 ratio, with the test set randomly assigned. The training and validation sets were stratified based on binned RPA values to ensure similar distribution across both sets. Affinity and non-affinity samples were defined using an RPA threshold of 0.001%. Within each split, affinity samples were used for training, validation, or testing in the regression task.

To evaluate the model's generalizability to unseen data, a new literature search was conducted on April 27, 2025, using the same set of search terms. Previously retrieved articles were excluded, and data were extracted from the newly identified studies using the same pipeline. No imputation was applied; only the raw, directly extractable data were retained. In total, 0.46 million samples and 10.4 thousand proteins were collected, including over 3.6 thousand proteins not present in the original dataset.

Performance of established foundation models

Previous studies have demonstrated that tabular modality data can be used to predict the affinity of specific proteins to various nanomaterial treatments⁹, and that the physicochemical properties of protein sequences alone can be employed to predict their affinity to specific nanomaterials¹³. However, the representational capacity of tabular feature is limited. Categorical variables such as nanomaterial type and incubation source are difficult to generalize to unseen categories. Besides, heterogeneous data are challenging to handle; for instance, samples with magnetic separation protocols lack centrifugation parameters, and numerical features may be expressed in diverse units (e.g., concentration in mg/L vs. mol/L, or centrifugation speed in g vs. rpm) even different format (e.g. multiple time intervals with different feature values). Besides, traditional machine learning models, such as the widely used RF, often perform well on data drawn from the same distribution²⁸, but show limited generalization to unseen samples. As their learning process relies entirely on the observed training data, they

struggle to handle previously unseen inputs or samples with missing values.

To enhance the model's ability to process heterogeneous tabular data and improve generalization to unseen conditions, we leveraged protein- and text-based pretrained models (ESM2¹⁴ and Linq-Embed-Mistral¹⁶) to learn generalizable representations across both protein and tabular modalities (Fig. 1b). Furthermore, to facilitate interaction between different modalities, we adopted a multimodal fusion framework based on multi-head cross-attention mechanism²⁹. Classification and regression foundation models were constructed separately on the filled-only dataset and the merged dataset.

The performance of established models is shown in Fig. 3. Foundation models trained on the filled-only dataset exhibit strong performance when evaluated on the filled test set (Fig. 3a-b), achieving an accuracy of 0.89, an F1 score of 0.84, and an AUC (area under the curve) score of 0.96 for the classification task, along with an R^2 of 0.87 and an MAE of 0.52 for regression. However, their performance declines substantially on the raw (unfilled) test set, with classification accuracy dropping to 0.66, the F1 score to 0.61, and the AUC score to 0.79. Notably, recall remains relatively high at 0.82, suggesting that while the model can still identify most positive samples, its overall predictive capability deteriorates in the presence of missing values. Similarly, regression performance on the raw test set shows a marked decrease, with R^2 reducing to 0.45 and MAE increasing to 1.21, indicating poor generalization to incomplete or heterogeneous inputs.

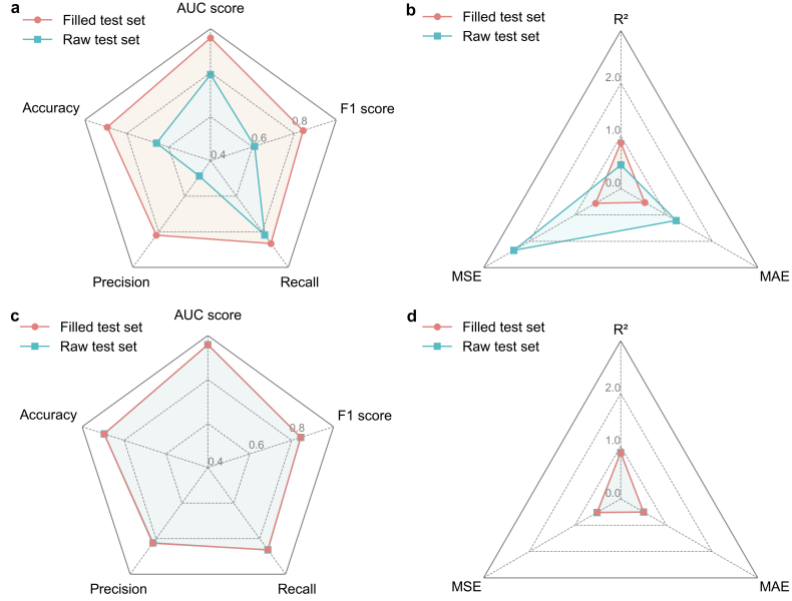


Fig. 3: Performance assessment of established foundation models on filled test set and raw test set. (a) Classification and (b) regression performance of foundation models built on the filled-only dataset. (c) Classification and (d) regression performance of foundation models built on the merged dataset. AUC, area under the curve. MSE, mean squared error. MAE, mean absolute error.

In contrast, foundation models trained on the merged dataset, containing both filled and unfilled samples, demonstrated consistently strong performance across both test sets (Fig. 3c-d). Classification metrics remains high on both the filled (accuracy: 0.90, F1 score: 0.84, AUC score: 0.96) and raw (accuracy: 0.89, F1 score: 0.84, AUC score: 0.96) test sets. Regression performance is similarly robust, with R^2 values of 0.88 on the filled and raw test sets. These results suggest that incorporating unfilled data (raw data) during training enhances the model's capacity to generalize to samples with missing or partially observed features, thereby improving reliability in real-world applications. Consequently, the foundation models trained on the merged dataset are selected for subsequent importance assessment and downstream applications.

Ablation-based modality and feature importance

Although protein and text-based pretrained large models offer enhanced generalization

capabilities, their vast parameter space, involving billions of parameters, renders model behavior increasingly opaque^{30,31}. Nevertheless, providing a certain degree of explainability remains essential. Explainability not only allows for the verification of whether the model has captured meaningful biological or physicochemical patterns, thereby enhancing trust and transparency, but also enables the extraction of domain-specific insights from the learned representations. Therefore, we employed an ablation-based importance analysis to evaluate the contribution of different modalities, the significance of individual tabular features, and their potential interactions (Fig. 4). This approach enables a systematic assessment of which components of the input, such as protein embeddings, experimental conditions, or specific physicochemical parameters, are most influential in driving the model's predictions.

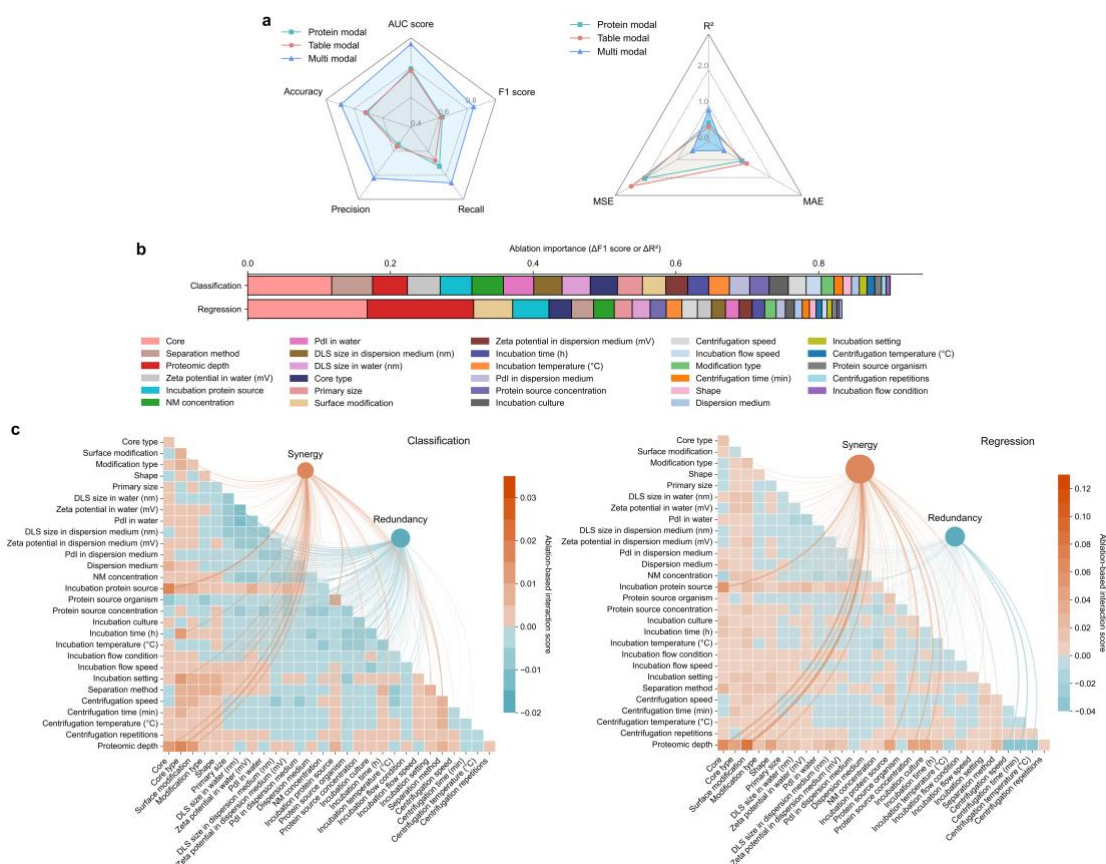


Fig. 4: Ablation-based importance of modals and features. (a) Modal importance. (b) Feature importance. (c) Feature interactions. The width and color intensity of the lines in (c) are proportional to the magnitude of the interaction effects. Note that the

scaling coefficients differ between the two subplots to enhance visual clarity. However, the point size of synergy and redundancy are scaled consistently in each subplot to facilitate a more effective comparison.

Modality ablation reveals that foundation models trained using either protein sequences or tabular descriptors alone achieve comparable performance in both classification and regression tasks, with protein-based models exhibiting a slight advantage (Fig. 4a). As expected, models integrating both modalities substantially outperform their single-modality counterparts, emphasizing the critical value of jointly leveraging protein-level biochemical representations and structured experimental context. Nevertheless, multimodal interactions, regardless of implementation strategy, remain among the least explored aspects in current research.

For the tabular modality, individual feature ablation results are shown in Fig. 4b. Among all features, the nanomaterials' core composition emerges as the most influential predictor across both classification and regression models. It is well-known that surface chemistry of nanomaterials is important factor influencing protein corona formation³². Among the top 12 most important features in the classification model, eight are related to the surface chemistry of nanomaterials, such as core composition, zeta potential, and polydispersity index (PDI). The remaining four are separation method, proteomic depth, nanomaterial concentration, and incubation protein source. Because the full dynamic process of nanomaterial-protein interactions is difficult to observe directly, what is typically analyzed is the protein corona isolated after the interaction has occurred. Consequently, experimental factors such as the separation method and the depth of proteomic analysis significantly affect the observed outcomes. For instance, centrifugation, the most widely used separation method, enables high-throughput processing, but can also alter the composition of the resulting protein corona³³. Its performance is influenced by parameters such as centrifugal force and the number of washing steps. Besides, corona composition characterization is highly dependent on

liquid chromatography-mass spectrometry (LC-MS). In a comparative study, analysis of the same sample by different core facilities yielded only 73 shared proteins out of 4,022 identified (1.8%), highlighting substantial variability across semiquantitative workflows⁷. These procedural details, though often considered technical, have a direct impact on the observed interaction profiles between nanomaterials and proteins, and thus must be carefully considered when interpreting proteomic results. These features are therefore not merely technical details, but critical determinants of how accurately and sensitively the protein corona can be profiled. Furthermore, the concentration of nanomaterials controls the surface area available for protein binding, thereby influencing adsorption-desorption kinetics and the composition of the resulting corona³⁴; while the source of incubation proteins determines which proteins are available to interact with the nanomaterials. Notably, coarse-grained features appear sufficient for classification tasks, whereas regression requires finer contextual detail. For example, proteomic depth ranks third in classification but rises to second in regression, nearly matching the importance of nanomaterial core composition. This likely reflects its role in defining the analytical sensitivity of proteomic profiling, i.e., the depth to which low-abundance proteins can be reliably detected, which directly impacts the accuracy of quantitative protein abundance estimation.

To assess interaction effects between features, we also conduct pairwise ablation to quantify potential synergistic or redundant contributions between tabular features, offering insights into complex feature interdependencies in nanomaterial-protein interaction modeling (Fig. 4c). The results indicate that, in the classification model, redundancy dominates over synergy among feature pairs, whereas in the regression model, synergistic effects outweigh redundancy. This underscores the greater reliance of regression tasks on high-resolution input features and their coordinated interactions.

Zero-shot inference: performance and generalizability to unseen data

To evaluate the generalizability of the model to unseen data, we conducted assessments

on a held-out dataset collected from studies published after the construction of the merged dataset. This dataset comprises fifteen independent studies, including thirteen containing previously unseen proteins, five with unseen nanomaterial core compositions, three with unseen surface modifications, and seven with previously unobserved incubation protein sources. These studies were selected from the recently published literature based solely on data availability, without any subjective filtering, ensuring an objective and unbiased evaluation of model generalizability.

The performance results are shown in Fig. 5. The classification foundation model achieves an average performance exceeding 0.7 across all key metrics (accuracy, precision, recall, and F1 score) in the 15 external studies (Fig. 5a), indicating strong generalizability to unseen data. As shown in Fig. 5b, the model achieves an accuracy of 0.69 for negative samples ($RPA < 0.001\%$). For positive samples, both the predicted probability and accuracy increase with higher RPA values, while the variability of predicted probabilities decreases, indicating improved model stability at higher affinity levels. In contrast, the regression model exhibits notably poor predictive performance on the same external datasets ($R^2 < 0$). This discrepancy may stem from the inherently higher specificity required for regression tasks, which demand the accurate estimation of continuous affinity values. Moreover, variability in sample preparation, corona isolation, proteomic platforms, and quantification methods, makes cross-study RPA prediction highly challenging because the protein corona analysis result cannot be easily compared across independent studies⁷. Nevertheless, fine-tuning the regression foundation model offers an alternative path for accurate prediction in specific case, which is further discussed in the following section.

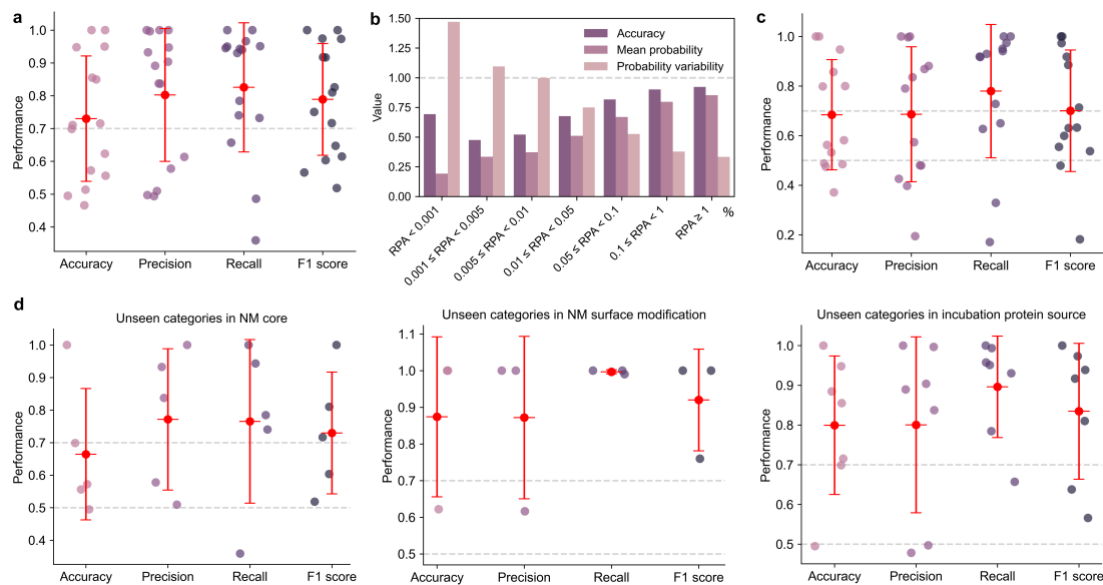


Fig. 5: Performance of the classification foundation model on unseen samples. (a) Performance on unseen samples from external studies. The AUC score was not reported because some studies only provided top-ranked proteins, resulting in datasets that contain only positive samples. (b) Accuracy, mean predicted probability, and probability variability across different RPA intervals. (c) Performance on unseen proteins derived from external studies. (d) Performance on samples with previously unseen categories in nanomaterial core composition, nanomaterial surface modification, and incubation protein source. In panels (a), (c), and (d), each point corresponds to an individual external study, with error bars denoting the mean \pm standard deviation.

The established foundation model also demonstrates acceptable predictive performance for previously unseen proteins and unseen categorical features within the tabular features. Specifically, its performance on unseen proteins approaches or exceeds 0.7 across all four metrics, indicating robust generalization. These results suggest that the use of protein- and text-based embedding models enables the capture of underlying structural and semantic information from both protein sequences and tabular features, beyond merely memorizing specific protein identities or categorical labels. This capability markedly surpasses that of traditional ML models, which often rely heavily on observed categories and struggle to generalize to unseen entities. The incorporation

of pretrained embeddings thus provides a substantial advantage in handling the heterogeneity and open-set nature of nanomaterial-protein interaction data.

Task-specific fine-tuning across four domains

In addition to the zero-shot application of the foundation models, their performance on specific tasks can be further improved through fine-tuning with a small amount of data. We selected four representative case studies, with sample sizes ranging from less than hundred to several hundred thousand, encompassing antibody binding³⁵, cell receptor³⁶, disease biomarker³⁷, and in-deep proteomic³⁸.

The classification and regression performances before and after fine-tuning are shown in Fig. 6. All four case studies exhibit improvements in AUC scores, ranging from 9.27% to 50.04%, with an average increase of 33.18%. The improvement in R^2 is even more pronounced, as the original foundation models show limited predictive ability in some cases. Following fine-tuning, the average R^2 across the four cases increases to 0.71. Despite these overall gains, both classification and regression models show relatively modest performance in the case of cell surface receptors (Fig. 6b). This may be partially attributed to characteristics specific to this study. Notably, 62% of the proteins involved in this task were not present in the training set, which likely limited the model's generalizability. In addition, unlike plasma or serum proteins that interact directly with nanomaterials, cell surface receptors engage with the protein corona after its initial formation, representing a secondary layer of interaction. Such interactions may involve distinct biophysical mechanisms and greater biological heterogeneity, further complicating predictive modeling. Additionally, the substantial improvement observed on in-depth proteomic study, shown in Fig. 6d, demonstrates the model's applicability as proteomic technologies advance and enable the detection of increasingly comprehensive protein repertoires.

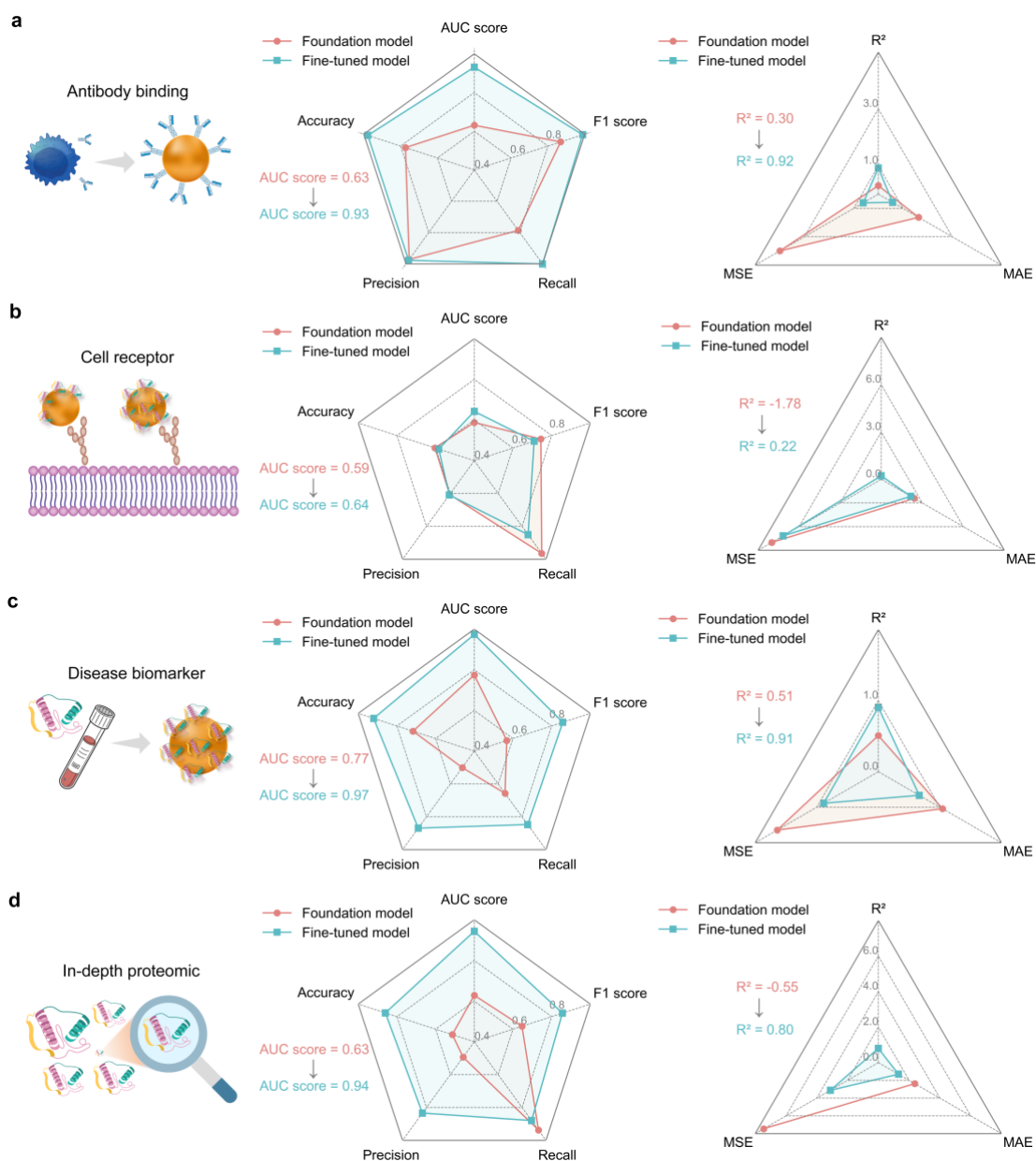


Fig. 6: Fine-tuning applications on four specific tasks. (a) Antibody binding. (b) Cell receptor. (c) Disease biomarker. (d) In-depth proteomic.

Discussion

Nanomaterials hold great promise in diagnostics and therapies due to their unique advantages in drug delivery³⁹, imaging⁴⁰, and theranostics⁴¹. Understanding nanomaterial-protein interactions is essential for advancing nanomedicine and ensuring nanomaterial safety in biomedical and environmental contexts⁴. However, the vast combinatorial space of nanomaterials and proteins, combined with sparse data and

complex experimental systems, has limited progress in the field. Investigating nanomaterial-protein corona formation solely through experimental approaches remains time-consuming and resource-intensive⁴², and conclusions drawn from limited datasets are often difficult to generalize across systems⁴³. Existing AI studies often focus on narrow, predefined scenarios, restricting generalizability. Notably, the current state of AI in nanomaterial-protein interaction research resembles the period before the introduction of ImageNet in computer vision, when methodological innovation was constrained by limited and fragmented datasets. Just as ImageNet catalyzed a leap in model capabilities by providing a large-scale, standardized benchmark⁴⁴, a comprehensive dataset is essential to fully realize the potential of modern AI methods in this domain. To address this, we construct NanoPro-3M, the largest dataset in protein corona research to date, encompassing over 3.2 million samples and 37,000 unique proteins. This dataset serves as the ImageNet for nanomaterial-protein interactions, enabling systematic exploration of these complex interfaces at unprecedented scale.

As noted earlier, prior studies have typically investigated unidirectional relationships, either how nanomaterials influence a specific protein, or vice versa. In contrast, our foundation model, built on million pairs of protein sequences and tabular features, demonstrates strong predictive performance across incomplete data and unseen categories. This highlights its value for high-throughput screening and efficient nanomaterial design. While the model’s generalization in regression tasks remains limited, its solid performance on internal test sets indicates effective learning capacity, with cross-study heterogeneity⁷ likely constraining fine-grained prediction. Notably, the model can be effectively fine-tuned with minimal data to improve task-specific performance—an essential feature given the pronounced heterogeneity across studies. This allows the model to learn fundamental patterns from large-scale datasets while adapting flexibly to individual experimental contexts.

To enhance model explainability and build trust in its predictions, we employ the ablation-based measurement method to quantify the relative importance of input modalities and individual features. These evaluations highlight the critical role of integrating both protein-level representations and structured experimental metadata for accurately modeling nanomaterial-protein interactions, an aspect largely overlooked in current research. Additionally, the analysis of tabular feature importance and interactions offers mechanistic insights into the model’s decision-making process. The alignment between key features and established domain knowledge supports the model’s reliability, while also identifying critical factors in nanomaterial-protein interactions as revealed by our model trained on the largest dataset to date.

Together, our dataset and model provide a robust foundation for generalizable and scalable prediction of nanomaterial-protein interactions. Future work may focus on the underexplored “dark space” of proteomics—proteins that are rarely studied⁴⁵ but may play critical roles in biological processes or serve as biomarkers. While our model shows promising generalization to these proteins, further performance improvements will require targeted data augmentation. Additionally, this approach has the potential to significantly accelerate *in vitro* nanomaterial-protein research by reducing reliance on time-consuming and costly experiments, enabling reliable predictions with minimal experiments. For researchers with AI expertise seeking to further improve model performance, promising directions include exploring alternative model architectures and pretraining strategies, incorporating information of protein structure and molecule structure using graph neural network⁴⁶, integrating domain knowledge, and enhancing model explainability.

While NanoPro-3M represents the most comprehensive dataset to date for nanomaterial-protein interactions, and NanoProFormer may be the first generalizable model capable of predicting interactions between arbitrary nanomaterials and proteins, we acknowledge its current limitations. Specifically, the dataset and model focus on the

post-interaction phase, a relatively tractable experimental endpoint that does not capture the intrinsically dynamic, non-equilibrium nature of nano-bio interactions *in vivo*. In physiological environments, biomolecular corona formation is a kinetic, multistep process involving initial diffusion to the nanomaterial surface followed by competitive and sequential biomolecule exchange⁴⁷. Proteins that first associate with the bare surface may later be displaced as secondary interactions, such as protein-protein associations and surface curvature effects-gain prominence. These dynamic adsorption events are influenced not only by medium composition but also by adsorption sequence and nanoscale geometry, resulting in corona profiles that deviate markedly from classical macroscopic phenomena such as the Vroman effect. Consequently, nanomaterials can selectively enrich rare or unexpected biomolecules from complex biofluids. We suggest that experimental resources currently focused on static observations could be more effectively redirected toward investigating adsorption-desorption kinetics, which is critical for advancing *in vivo* applications of nanomaterials.

Nevertheless, the present work holds significant practical relevance, particularly for post-interaction-based applications such as early and rapid disease diagnostics. Owing to their relative stability and experimental accessibility, hard coronas are widely utilized as a major element of the biological identity of nanomaterials and as a means to target diseases⁴⁸. In clinical settings, where target signals are sparse and embedded in complex biological matrices, the ability to engineer nanomaterials that selectively enrich specific protein biomarkers is particularly valuable. Sparse protein models even outperformed those using basic features and clinical assay data across 52 diseases⁴⁹. Protein adsorption onto nanomaterial surfaces can elicit detectable changes in physicochemical properties, enabling biosensing applications for static detection of disease-relevant signatures⁵⁰. Our dataset and model lay a foundation for zero-shot screening, rational nanomaterial design, and broader deployment in static interaction scenarios, including biosensor development and nano-bio interface engineering—thereby accelerating the

translation of nanomaterials into real-world applications.

In summary, we present NanoPro-3M, a million-scale, multimodal dataset that captures the complexity of nanomaterial-protein interactions, alongside NanoProFormer, a cross-modal foundation model that jointly encodes protein sequences and structured nanomaterial descriptors with robust and generalizable predictive capabilities. Through importance analyses, we underscore the critical role of multimodal integration and reveal key determinants of model behavior, enhancing explainability and trust. Our approach helps mitigate the need for costly and time-consuming experimental procedures, offering a foundation for static investigations of nanomaterial-protein interactions and enabling scalable *in vitro* applications such as disease diagnostics. Looking forward, we envision exciting opportunities at the intersection of AI and nanobiotechnology—ranging from the incorporation of structural priors and expert knowledge, to the design of novel architectures and pretraining paradigms aimed at improving model generalization and explainability. Importantly, we advocate that experimental resources saved from static assays be reallocated to investigating dynamic interaction processes—a vital step toward temporally-aware modeling and *in vivo* translation of nanomaterials.

Methods

In this section, together with relevant sections in the Supplementary Information, we explain the technical details of data collection (Supplementary Section 1), dataset curation (Supplementary Section 2), embedding acquisition (Supplementary Section 3), model establishment (Supplementary Section 4), importance assessment (Supplementary Section 5), and applications of foundation models (Supplementary Section 6).

Data collection

As of September 20, 2024, we conducted a comprehensive literature search across Web of Science, PubMed, and Scopus, focusing exclusively on original research articles. Duplicate entries were removed based on DOI, followed by the exclusion of articles with insufficient text length or low citation counts (adjusted by publication year). Keyword-based filtering was applied to retain studies containing relevant terms such as mass spectrometry, abundance quantification or spectral analysis, and data table. Fully manual data extraction is highly labor-intensive, whereas LLMs offer a new and efficient approach to streamline this process²³. Subsequently, aided by LLMs with tailored prompts⁵¹, we extracted structured experimental descriptors from the filtered articles, which were then manually verified. A total of 29 features were curated, including 14 describing nanomaterial properties, 9 related to incubation conditions, 5 detailing separation protocols, and 1 capturing a key proteomic analysis setting. All extracted numerical values were cross-checked against the original publications for accuracy. To assess the model’s generalizability to unseen data, a second literature search was performed on April 27, 2025, using the same search strategy. Previously identified articles were excluded, and structured data were extracted from the newly identified studies using the same semi-automated pipeline.

Dataset curation

In addition to basic preprocessing steps such as standardizing capitalization, units, and removing redundant whitespace, we performed extensive semantic alignment, data cleaning, and imputation to ensure the consistency and usability of the dataset. For semantic alignment, we standardized nomenclature across multiple features. For instance, in the category of nanomaterial core, entries such as “carbon nanotubes” and “GO” were aligned to “carbon” to preserve the structural information in the shape feature and avoid redundancy across fields. Core compositions like “Au and Fe₃O₄” were standardized to “Au@Fe₃O₄.” All core types were harmonized into seven overarching categories: metal-based, metal oxide-based, carbon-based, polymer-based, lipid-based, core-shell, and other. Surface modifications presented greater semantic

variability. To systematically standardize them, we first constructed a domain-specific knowledge vector database from the retrieved corpus. This was followed by vector-based retrieval and inference using retrieval-augmented reasoning LLMs^{52,53} to identify common surface modification names and classify them into charge-based categories (Anionic, Neutral, Cationic). For the shape attribute, all terms were mapped to one of six categories: spherical, rod-like, sheet-like, plate-like, polyhedral, and complex. Primary size was standardized in nanometers (nm), and different geometric forms were treated accordingly, for instance, spherical particles with a single dimension versus rod-like or sheet-like materials with both diameter and length specified (e.g., “diameter 80, length 1500”). Missing values for primary size were estimated using weighted averages within grouped categories defined by core composition, core type, surface modification, modification type, and particle shape. Polydispersity index (PdI) and concentration were imputed using the same strategy, ensuring consistency across structurally and chemically similar nanomaterials. For dynamic light scattering (DLS) size and zeta potential, imputation was guided by a combination of contextual chemical properties and LLM-based inference trained on prior examples²⁵. In cases where the dispersing medium was not specified, we assumed water as the default. Concentration values were unified to mg/L when conversion was possible, while other units such as wt% and m²/mL were retained with appropriate standardization. For missing values in protein incubation or separation protocols, most were imputed using the mode of the respective feature, for example, Incubation temperature was defaulted to 37 °C. Data imputation was performed only on the dataset used for model training. For the unseen evaluation dataset, only basic preprocessing steps such as semantic alignment were applied, and missing values were left unfilled to assess the model’s generalization ability under real-world conditions.

Due to inconsistencies in reported RPA values across studies, we estimated RPA based on available quantification-related data using normalization, molecular weight-based normalization, or the iBAQ⁵⁴ methods, such as RPA⁵⁵, spectral count⁵⁶, intensity⁵⁷,

peptide number⁵⁸, molar masses⁵⁹, and emPAI⁶⁰. For studies reporting multiple experimental groups, protein counts were summed across groups. Proteins absent in specific groups were assigned an RPA of zero (termed "local fill"). For studies that reported only the top-ranked proteins with RPA values summing to one, we applied top-n proportional scaling. Specifically, we first computed the typical cumulative abundance of the top-ranked proteins from studies with complete protein profiles. Based on this reference, we proportionally scaled the reported abundances in studies that listed no more than 150 proteins. We then performed a "global fill" for proteins detected in over 10% of samples and three studies. For classification tasks, we binarized protein presence using a threshold of 0.001% RPA, assigning 1 to values above the threshold and 0 otherwise. For regression tasks, given the highly skewed, long-tailed distribution of RPA values, we applied a Box-Cox transformation to stabilize variance and approximate normality.

Embedding acquisition

We leveraged protein- and text-based pretrained models (ESM2¹⁴ and Linq-Embed-Mistral¹⁶, both of which were state-of-the-art models), which have been trained on massive datasets and have captured a broad range of underlying patterns, enabling them to learn highly generalizable representations across both protein and tabular modalities. For protein-based pretrained models, we simply inputted the amino acid sequence into ESM2_t36_3B_UR50D to obtain a 2560-dimensional representation vector. For text-based pretrained models, we designed prompt incorporating task description, background information, and contextual knowledge. By filling sample-specific numerical values into the designed prompt, we obtained 4096-dimensional representation vectors. Inference with large models is time-intensive; therefore, we pre-encoded all unique tabular descriptors and protein sequences to avoid redundant computation for repeated inputs.

Model establishment

Based on the pretrained embeddings described above, we designed a streamlined model architecture comprising three components: a projection module, a cross-modal fusion module, and a prediction module. The protein- and text-based embeddings were first projected into a shared latent space of 1024 dimensions via two separate projection modules. These representations were then integrated using a multi-head cross-attention mechanism, enabling effective fusion of modality-specific information. Finally, a multilayer perceptron was used to map the fused representation to the target prediction. To address class imbalance in the classification task, particularly the underrepresentation of positive samples, we applied a weighting strategy that increased the relative importance of positive examples. Specifically, the loss function assigned a weight to positive samples equivalent to twice the ratio of negative to positive instances, reflecting the practical need to prioritize the correct identification of positive cases, even at the cost of tolerating some false positives.

Importance assessment

We employed an ablation-based approach to assess the contributions of each modality and individual features to model performance. For modality ablation, we trained models using only one modality, either protein embeddings or tabular features, on the same dataset. These models followed an architecture nearly identical to the full model, except that the cross-attention module was replaced with a self-attention mechanism. For the tabular modality, we conducted feature ablation by setting the value of each feature to "Unknown" and re-encoding the input using the same text encoder. Performance degradation on the test set was then measured using the F1 score for classification tasks and the R^2 metric for regression. To evaluate feature interaction effects, we extended the ablation to feature pairs: two features were simultaneously masked as "Unknown," and the observed performance loss was compared to the sum of losses from individual feature ablations.

Applications of the foundation models

The foundation model was utilized in two ways: zero-shot inference and task-specific fine-tuning. For zero-shot inference, new samples were encoded using the same pretrained models. In the case of the text modality, structured prompts were applied prior to encoding. The resulting representation vectors were then directly fed into the pretrained foundation model for prediction. For fine-tuning, we sought to enhance model performance on specific tasks using a small number of labeled samples. Protein sequences and tabular descriptors were encoded using the same pretrained encoders. During fine-tuning, we froze the projection layers and cross-modality fusion module, and trained only the prediction head. The dataset was split into training, validation, and test sets in a 70:15:15 ratio.

References

1. Doane, T. L. & Burda, C. The unique role of nanoparticles in nanomedicine: imaging, drug delivery and therapy. *Chem. Soc. Rev.* **41**, 2885 (2012).
2. Kah, M., Tufenkji, N. & White, J. C. Nano-enabled strategies to enhance crop nutrition and protection. *Nat. Nanotechnol.* **14**, 532–540 (2019).
3. Huang, X. *et al.* Trends, risks and opportunities in environmental nanotechnology. *Nat. Rev. Earth Environ.* **5**, 572–587 (2024).
4. Mahmoudi, M., Landry, M. P., Moore, A. & Coreas, R. The protein corona from nanomedicine to environmental science. *Nat. Rev. Mater.* **8**, 422–438 (2023).
5. Blume, J. E. *et al.* Rapid, deep and precise profiling of the plasma proteome with multi-nanoparticle protein corona. *Nat. Commun.* **11**, 3662 (2020).
6. Hadjidemetriou, M., Mahmoudi, M. & Kostarelos, K. In vivo biomolecule corona and the transformation of a foe into an ally for nanomedicine. *Nat. Rev. Mater.* **9**, 219–222 (2024).
7. Ashkarran, A. A. *et al.* Measurements of heterogeneity in proteomics analysis of the nanoparticle protein corona across core facilities. *Nat. Commun.* **13**, 6610 (2022).
8. Zhang, P. *et al.* Analysis of nanomaterial biocoronas in biological and environmental surroundings. *Nat. Protoc.* **19**, 3000–3047 (2024).
9. Findlay, M. R., Freitas, D. N., Mobed-Miremadi, M. & Wheeler, K. E. Machine learning provides predictive analysis into silver nanoparticle protein corona formation from physicochemical properties. *Environ. Sci. Nano* **5**, 64–71 (2018).
10. Ban, Z. *et al.* Machine learning predicts the functional composition of the protein corona and the cellular recognition of nanoparticles. *Proc. Natl. Acad. Sci.* **117**, 10492–10499 (2020).
11. Fu, X. *et al.* Machine Learning Enables Comprehensive Prediction of the Relative Protein Abundance of Multiple Proteins on the Protein Corona. *Research* **7**, 0487 (2024).
12. Su, Y. *et al.* PROTCROWN: A Manually Curated Resource of Protein Corona Data for Unlocking the Potential of Protein–Nanoparticle Interactions. *Nano Lett.* **25**, 1739–1744 (2025).
13. Ouassil, N., Pinals, R. L., Del Bonis-O'Donnell, J. T., Wang, J. W. & Landry, M. P. Supervised learning model predicts protein adsorption to carbon nanotubes. *Sci. Adv.* **8**, eabm0898 (2022).
14. Lin, Z. *et al.* Evolutionary-scale prediction of atomic-level protein structure with a language

- model. *Science* **379**, 1123–1130 (2023).
15. Abramson, J. *et al.* Accurate structure prediction of biomolecular interactions with AlphaFold 3. *Nature* **630**, 493–500 (2024).
 16. Choi, C. *et al.* Linq-Embed-Mistral Technical Report. Preprint at <https://doi.org/10.48550/ARXIV.2412.03223> (2024).
 17. Devlin, J., Chang, M.-W., Lee, K. & Toutanova, K. BERT: Pre-training of Deep Bidirectional Transformers for Language Understanding. in *Proceedings of the 2019 Conference of the North American Chapter of the Association for Computational Linguistics: Human Language Technologies, Volume 1 (Long and Short Papers)* (eds. Burstein, J., Doran, C. & Solorio, T.) 4171–4186 (Association for Computational Linguistics, Minneapolis, Minnesota, 2019). doi:10.18653/v1/N19-1423.
 18. Jumper, J. *et al.* Highly accurate protein structure prediction with AlphaFold. *Nature* **596**, 583–589 (2021).
 19. Unsal, S. *et al.* Learning functional properties of proteins with language models. *Nat. Mach. Intell.* **4**, 227–245 (2022).
 20. Madani, A. *et al.* Large language models generate functional protein sequences across diverse families. *Nat. Biotechnol.* **41**, 1099–1106 (2023).
 21. Zeng, Z., Yao, Y., Liu, Z. & Sun, M. A deep-learning system bridging molecule structure and biomedical text with comprehension comparable to human professionals. *Nat. Commun.* **13**, 862 (2022).
 22. Jiang, X. *et al.* Applications of natural language processing and large language models in materials discovery. *Npj Comput. Mater.* **11**, 79 (2025).
 23. Dagdelen, J. *et al.* Structured information extraction from scientific text with large language models. *Nat. Commun.* **15**, 1418 (2024).
 24. Reed, S. M. Augmented and Programmatically Optimized LLM Prompts Reduce Chemical Hallucinations. *J. Chem. Inf. Model.* **65**, 4274–4280 (2025).
 25. Brown, T. B. *et al.* Language Models are Few-Shot Learners. Preprint at <https://doi.org/10.48550/ARXIV.2005.14165> (2020).
 26. Tordjman, M. *et al.* Comparative benchmarking of the DeepSeek large language model on

- medical tasks and clinical reasoning. *Nat. Med.* (2025) doi:10.1038/s41591-025-03726-3.
27. The UniProt Consortium *et al.* UniProt: the Universal Protein Knowledgebase in 2025. *Nucleic Acids Res.* **53**, D609–D617 (2025).
 28. Grinsztajn, L., Oyallon, E. & Varoquaux, G. Why do tree-based models still outperform deep learning on typical tabular data? in *Advances in Neural Information Processing Systems* (eds. Koyejo, S. et al.) vol. 35 507–520 (Curran Associates, Inc., 2022).
 29. Vaswani, A. *et al.* Attention Is All You Need. Preprint at <https://doi.org/10.48550/ARXIV.1706.03762> (2017).
 30. Boselli, R., D’Amico, S. & Nobani, N. eXplainable AI for Word Embeddings: A Survey. *Cogn. Comput.* **17**, 19 (2025).
 31. Vu, M. H. *et al.* Linguistically inspired roadmap for building biologically reliable protein language models. *Nat. Mach. Intell.* **5**, 485–496 (2023).
 32. Bilardo, R., Traldi, F., Vdovchenko, A. & Resmini, M. Influence of surface chemistry and morphology of nanoparticles on protein corona formation. *WIREs Nanomedicine Nanobiotechnology* **14**, (2022).
 33. Sun, Y., Zhou, Y., Rehman, M., Wang, Y.-F. & Guo, S. Protein Corona of Nanoparticles: Isolation and Analysis. *Chem Bio Eng.* **1**, 757–772 (2024).
 34. García-Álvarez, R. & Vallet-Regí, M. Hard and Soft Protein Corona of Nanomaterials: Analysis and Relevance. *Nanomaterials* **11**, 888 (2021).
 35. Yoo, J. *et al.* Surface-engineered nanobeads for regiospecific antibody binding: A robust immunoassay platform leveraging catalytic signal amplification. *Biosens. Bioelectron.* **281**, 117463 (2025).
 36. Baimanov, D. *et al.* Identification of Cell Receptors Responsible for Recognition and Binding of Lipid Nanoparticles. *J. Am. Chem. Soc.* **147**, 7604–7616 (2025).
 37. Guha, A. *et al.* AI-driven prediction of cardio-oncology biomarkers through protein corona analysis. *Chem. Eng. J.* **509**, 161134 (2025).
 38. Liu, Q. *et al.* Extreme Tolerance of Nanoparticle-Protein Corona to Ultra-High Abundance Proteins Enhances the Depth of Serum Proteomics. *Adv. Sci.* **12**, 2413713 (2025).
 39. Mitchell, M. J. *et al.* Engineering precision nanoparticles for drug delivery. *Nat. Rev. Drug*

- Discov.* **20**, 101–124 (2021).
40. Hsu, J. C. *et al.* Nanomaterial-based contrast agents. *Nat. Rev. Methods Primer* **3**, 30 (2023).
 41. Chen, W. *et al.* Macrophage-targeted nanomedicine for the diagnosis and treatment of atherosclerosis. *Nat. Rev. Cardiol.* **19**, 228–249 (2022).
 42. Hasenkopf, I. *et al.* Computational prediction and experimental analysis of the nanoparticle-protein corona: Showcasing an in vitro-in silico workflow providing FAIR data. *Nano Today* **46**, 101561 (2022).
 43. Pino, P. D. *et al.* Protein corona formation around nanoparticles – from the past to the future. *Mater Horiz* **1**, 301–313 (2014).
 44. Deng, J. *et al.* ImageNet: A large-scale hierarchical image database. in *2009 IEEE Conference on Computer Vision and Pattern Recognition* 248–255 (IEEE, Miami, FL, 2009). doi:10.1109/CVPR.2009.5206848.
 45. Kustatscher, G. *et al.* Understudied proteins: opportunities and challenges for functional proteomics. *Nat. Methods* **19**, 774–779 (2022).
 46. Corso, G., Stark, H., Jegelka, S., Jaakkola, T. & Barzilay, R. Graph neural networks. *Nat. Rev. Methods Primer* **4**, (2024).
 47. Dawson, K. A. & Yan, Y. Current understanding of biological identity at the nanoscale and future prospects. *Nat. Nanotechnol.* **16**, 229–242 (2021).
 48. Monopoli, M. P., Åberg, C., Salvati, A. & Dawson, K. A. Biomolecular coronas provide the biological identity of nanosized materials. *Nat. Nanotechnol.* **7**, 779–786 (2012).
 49. Carrasco-Zanini, J. *et al.* Proteomic signatures improve risk prediction for common and rare diseases. *Nat. Med.* **30**, 2489–2498 (2024).
 50. Welch, E. C., Powell, J. M., Clevinger, T. B., Fairman, A. E. & Shukla, A. Advances in Biosensors and Diagnostic Technologies Using Nanostructures and Nanomaterials. *Adv. Funct. Mater.* **31**, (2021).
 51. Chen, B., Zhang, Z., Langrené, N. & Zhu, S. Unleashing the potential of prompt engineering for large language models. *Patterns* **6**, 101260 (2025).
 52. Gao, Y. *et al.* Retrieval-Augmented Generation for Large Language Models: A Survey. Preprint at <https://doi.org/10.48550/ARXIV.2312.10997> (2023).

53. Hou, Z. *et al.* Advancing Language Model Reasoning through Reinforcement Learning and Inference Scaling. Preprint at <https://doi.org/10.48550/ARXIV.2501.11651> (2025).
54. Schwanhäusser, B. *et al.* Global quantification of mammalian gene expression control. *Nature* **473**, 337–342 (2011).
55. Yu, L. *et al.* Enhanced Cancer-targeted Drug Delivery Using Precoated Nanoparticles. *Nano Lett.* **20**, 8903–8911 (2020).
56. Marques, C. *et al.* Identification of the Proteins Determining the Blood Circulation Time of Nanoparticles. *ACS Nano* **17**, 12458–12470 (2023).
57. Ferdosi, S. *et al.* Enhanced Competition at the Nano–Bio Interface Enables Comprehensive Characterization of Protein Corona Dynamics and Deep Coverage of Proteomes. *Adv. Mater.* **34**, 2206008 (2022).
58. Chen, F. *et al.* Complement proteins bind to nanoparticle protein corona and undergo dynamic exchange in vivo. *Nat. Nanotechnol.* **12**, 387–393 (2017).
59. Madathiparambil Visalakshan, R. *et al.* The Influence of Nanoparticle Shape on Protein Corona Formation. *Small* **16**, 2000285 (2020).
60. Mirshafiee, V., Kim, R., Mahmoudi, M. & Kraft, M. L. The importance of selecting a proper biological milieu for protein corona analysis in vitro: Human plasma versus human serum. *Int. J. Biochem. Cell Biol.* **75**, 188–195 (2016).

Data availability

The curated datasets will be made publicly and unconditionally available upon acceptance of the manuscript.

Code availability

Codes for embedding acquisition, model establishment, and importance assessment are available at <https://github.com/YuHengjie/NanoProFormer-public>. Codes for model inference and fine-tuning as well as foundation models are available at <https://github.com/YuHengjie/NanoProFormer-Zero-shot> with detailed instructions.

Author contributions

H.Yu and Y.J. conceived the study. H.Yu, H.Yang, and S.L. collected and curated the data. H.Yu implemented the code and performed the analyses. K.A.D., Y.Y., and Y.J. revised the manuscript. Y.J. and H.Yu acquired funding. All authors discussed the results and approved the final manuscript.

Acknowledgements

This work is supported by International Collaboration Fund for Creative Research Teams of National Natural Science Foundation of China (grant No. W2441019), Westlake Education Foundation (grant No. 103110846022301), and China Postdoctoral Science Foundation (grant No. 2024M762941).

Competing interests

H.Yu and Y. J. have filed patent applications covering the work presented. The other authors declare no competing interests.